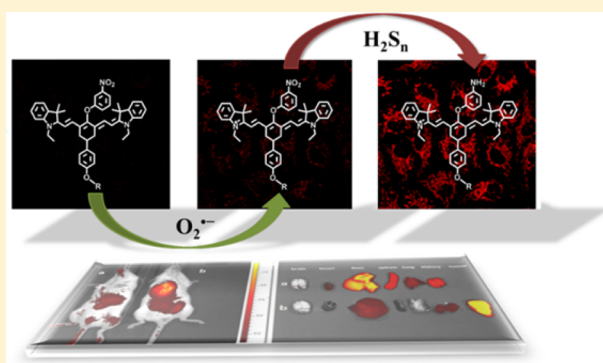


Near-Infrared Fluorescence Probe for in Situ Detection of Superoxide Anion and Hydrogen Polysulfides in Mitochondrial Oxidative Stress

Yan Huang,^{†,‡} Fabiao Yu,^{*,†} Jianchao Wang,[‡] and Lingxin Chen^{*,†,§}[†]Key Laboratory of Coastal Environmental Processes and Ecological Remediation, Yantai Institute of Coastal Zone Research, Chinese Academy of Sciences, Yantai 264003, China[‡]Department of Chemistry, Qinghai Normal University, Xining 810008, China[§]College of Life Science, Yantai University, Yantai 264005, China

Supporting Information

ABSTRACT: H₂S plays important physiological and pathological roles in the cardiovascular system and nervous system. However, recent evidence imply that hydrogen polysulfides (H₂S_n) are the actual signaling molecules in cells. Although H₂S_n have been demonstrated to be responsible for mediating tumor suppressors, ion channels, and transcription factors, more of their biological effects are still need to be elaborated. On one hand, H₂S_n have been suggested to be generated from endogenous H₂S upon reaction with reactive oxygen species (ROS). On the other hand, H₂S_n derivatives are proposed to be a kind of direct antioxidant against intracellular oxidative stress. This conflicting results should be attributed to the regulation of redox homeostasis between ROS and H₂S_n. Superoxide anion (O₂^{•-}) is undoubtedly the primary ROS existing in mitochondria. We reason that the balance of O₂^{•-} and H₂S_n are pivotal in physiological and pathological processes. Herein, we report two near-infrared fluorescent probes Hcy-Mito and Hcy-Biot for the detection of O₂^{•-} and H₂S_n in cells and in vivo. Hcy-Mito is conceived to be applied in mitochondria, and Hcy-Biot is designed to target tumor tissue. Both of the probes were successfully applied for visualizing exogenous and endogenous O₂^{•-} and H₂S_n in living cells and in tumor mice models. The results demonstrate that H₂S_n can be promptly produced by mitochondrial oxidative stress. Flow cytometry assays for apoptosis suggest that H₂S_n play critical roles in antioxidant systems.



Reactive oxygen species (ROS) and reactive sulfur species (RSS) are endogenously widespread in cells. These species are involved in a wide range of physiological and pathological processes including cytoprotection, signal transduction, neurodegenerative injury, inflammation, and carcinogenesis.^{1–3} Since the prolonged exposure of ROS will potentially damage organelles, cells have developed several defense mechanisms, which comprise antioxidant enzymes and diametrically targeted elimination pathways. Therefore, the intracellular oxidative stress is interrelated with an imbalance between ROS production and cellular antioxidant capacity. Accumulated evidence suggest that hydrogen sulfide (H₂S, a member of RSS) plays essential roles in regulating the intracellular redox status and fundamental signaling processes.^{4,5} However, recently interests are focused on physiological functions of another member of RSS: hydrogen polysulfides (H₂S_n, $n > 1$).^{6–11} H₂S_n are composed of a combination of polysulfur molecules, which are inextricably balanced by H₂S oxygen-dependent catabolic processes in mitochondria.¹² Research results imply that H₂S_n behave the properties of antioxidant, cytoprotection, and redox signaling in tissues and organs,^{13–15} and H₂S may be the terminal product of H₂S_n when function in physical activity.^{16–18} The

endogenous H₂S can generate H₂S_n by reacting with ROS.^{8–10,19–21} However, H₂S_n derivatives are proposed to be direct antioxidants against ROS in cells.^{22,23} There is no doubt that H₂S_n possess their own biofunctions, but the evidence is limited owing to the lack of accurate and sensitive detection methods. We assume that these conflicting findings should be driven by the redox homeostasis between H₂S_n and ROS.

Superoxide anion (O₂^{•-}) is the primary one-electron reduced product from mitochondrial electron transport of the respiratory chain. It serves as the major source for other ROS.^{1,2} O₂^{•-} has long been recognized as a vital cellular signaling molecule involved in numbers of physiological processes from innate immunity to metabolic homeostasis. Nevertheless, excessive amounts of O₂^{•-} induces damages for biological membranes and tissues.^{24,25} The mitochondria fraction of H₂S_n and their derivatives are approximately up to 60%.^{26,27} We hypothesize that the mitochondrial redox state may have closed the relationship between H₂S_n and O₂^{•-}.

Received: February 2, 2016

Accepted: February 29, 2016

Published: February 29, 2016

Owing to their biological functions either in cells or in vivo, the elucidation of combined bioeffects of H_2S_n and $\text{O}_2^{\bullet-}$ have become an important area in research. The major obstacle for research is the rapid catabolism properties of both H_2S_n and $\text{O}_2^{\bullet-}$, which will result in the continuous fluctuations of their concentrations. Another challenge for the detection is that it is impossible to immediately separate H_2S_n and $\text{O}_2^{\bullet-}$ from biological systems. All these issues make it difficult to direct detection of H_2S_n and $\text{O}_2^{\bullet-}$ sensitively and selectively. A few methods have been developed for the detection of H_2S_n and $\text{O}_2^{\bullet-}$ including colorimetry,²⁸ electrochemical analysis,²⁹ and gas chromatography.³⁰ However, these technologies often require post-mortem processing and destruction of tissues or cells. Obviously, these technologies are not suitable for in real-time analysis of endogenous H_2S_n and $\text{O}_2^{\bullet-}$. Compared with these biological detection technologies, technology based on fluorescence probes for visualizing physiological and pathophysiological changes in cells has become increasingly indispensable, as this technology enables high sensitivity, superior selectivity, less invasion, more convenience, readily available instruments, as well as simple manipulation.^{1–3} Additionally, near-infrared (NIR) absorption and emission profiles can maximize tissue penetration while minimizing the absorbance of heme in hemoglobin and myoglobin, water, and lipids. Therefore, fluorescent probes that have NIR absorption and emission are preferential candidates for fluorescence imaging in cells and vivo.³¹ To date, the fluorescent probes for $\text{O}_2^{\bullet-}$ and H_2S_n separate detection have been elegantly developed.^{1,4} However, the combined-response fluorescent probes for in situ detection of $\text{O}_2^{\bullet-}$ and H_2S_n are urgently needed, because the crosstalk process between $\text{O}_2^{\bullet-}$ and H_2S_n includes signal transduction, homeostasis regulation, oxidative stress, and antioxidant repair in time in living cells. The integration of multiresponse to multispecies by a single probe can demonstrate the redox homeostasis process more clearly.^{32–39} Moreover, the multiresponse probes can benefit from inaccurate calibration. And they can also avoid photobleaching rates of individual probes, uneven probe loading, nonhomogeneous distribution uncontrollable localization, larger invasive effects, metabolisms, and interference of spectral overlap.^{34,39}

Herein, we conceived two new multiresponse fluorescent probes, Hcy-Mito and Hcy-Biot, for successively detecting the $\text{O}_2^{\bullet-}$ and H_2S_n in living cells and in vivo. The two probes could provide high sensitivity and selectivity toward $\text{O}_2^{\bullet-}$ and H_2S_n . Hcy-Mito was prioritized to image the redox homeostasis process between $\text{O}_2^{\bullet-}$ and H_2S_n in mitochondria. The results indicated that the burst of $\text{O}_2^{\bullet-}$ would induce the rapid generation of H_2S_n in cells. However, the excessive accumulation of $\text{O}_2^{\bullet-}$ could cause mitochondrial oxidative stress and induce cell apoptosis. Additionally, the application of Hcy-Biot in tumor-bearing mice (murine sarcoma S180) displayed that the probe could be located in cancerous tissue for the detection of $\text{O}_2^{\bullet-}$ and H_2S_n .

EXPERIMENTAL SECTION

Apoptosis Experiments. Human umbilical vein epithelial cells (HUVECs) were cultured at 2.0×10^5 cells/well in six-well plates and then treated as described in Figure 3. After harvest, cells were washed and suspended in 400 μL of Binding Buffer and then treated with 5 μL of Annexin V-FITC and 5 μL of Propidium Iodide for 10 min at 25 °C in dark. At last, the cells were analyzed by flow cytometry. Annexin V-FITC and

Propidium Iodide were detected by the green fluorescent channel and the red fluorescent channel, respectively.

Establishment of the Murine Sarcoma S180 Tumor.

S180 murine sarcoma cells were purchased from the Cell Preserve Center (Wuhan University, Wuhan, P.R. China). The culture flasks were covered with S180 murine sarcoma cells, and then we shifted the cells and cell culture medium to centrifuge tubes in a super clean bench. The cells were centrifuged at 1000 r/min for 10 min and discarded the supernatant. We adjusted the cell concentration by Hanks solution to cause S180 ascites tumor model. Six to eight-week-old BALB/C mice weighing about 20–25 g each were used. S180 murine sarcoma cells grown for 7 days in the ascites fluid of the mice were injected into an intracutaneous site on the right armpit of about 11-week-old mouse, at a dose of 0.2 mL of 3×10^6 /mL cells per site. The tumor-bearing mice received regular food, and the tumors were allowed to grow for about 8–10 days until the tumor diameter reached 8–10 mm.

Fluorescent Imaging of BALB/c Mice. BALB/c mice were obtained from Binzhou Medical University. Mice were group-housed on a 12:12 light-dark cycle at 22 °C with free access to food and water. BALB/c mice, 20–25 g, were selected and divided into different groups. Mice were anesthetized prior to injection and during imaging via inhalation of isoflurane. All the BALB/c mice were selected and divided into three groups. In the control group a, the peritoneal cavities of BALB/c mice were injected with 50 μL of 100 μM Hcy-Mito solution (DMSO/saline = 1:9, v/v). Group b were given i.p. cavity injection with Hcy-Mito for 20 min, and then injected with phorbol myristate acetate (PMA) 30 min to induce $\text{O}_2^{\bullet-}$ generation (50 nM, 50 μL in 1:99 DMSO/saline v/v). Group c were pre-treated as indicated in group b. Subsequently, these mice were given i.p. cavity injection with Na_2S_4 (50 μM , 100 μL in saline) for 30 min as the source of H_2S_n . At a time 20 min later, fluorescence images were constructed from fluorescence collection (750–850 nm, $\lambda_{\text{ex}} = 730$ nm) and using in vivo imaging system (Bruker). Additionally, we merged the fluorescence image with the corresponding X-ray image to clearly display the reaction site of the mice.

Fluorescent Imaging of Acute Hepatitis Mice and Sarcoma S180 BALB/c Mice. Sarcoma S180 BALB/c mice were group-housed on a 12:12 light-dark cycle at 22 °C with free access to food and water. We induced acute liver injury by D-galactosamine (D-GalN)/LPS in mice for the production of $\text{O}_2^{\bullet-}$ and H_2S_n . The mice in group a were intravenously injected with D-GalN/LPS (500 mg/kg and 50 $\mu\text{g}/\text{kg}$ LPS in saline) for 24 h. Subsequently, the mice were with intravenous injection of Hcy-Biot (1 μM , 50 μL in 1:99 DMSO/saline v/v) and maintained 1 h. The murine sarcoma S180 tumor bearing mice were injected intravenously with Hcy-Biot (1 μM , 50 μL in 1:99 DMSO/saline v/v) for 1 h. Images were taken by Xenogen IVIS Spectrum Preclinical In Vivo Imaging System.

RESULTS AND DISCUSSION

Design Strategies for Probes Hcy-Mito and Hcy-Biot.

The synthetic approaches of multiresponse fluorescence probes Hcy-Mito and Hcy-Biot were outlined in Scheme S1. The synthetic details of compounds were shown in the Supporting Information. The multiresponse mechanism for the probes was shown in Scheme 1. A heptamethine cyanine dye with NIR fluorescence emission was chosen as a fluorophore. Our desirable probes could be readily available from the versatile fluorophore. The reducibility of N^+ site in cyanine platform is

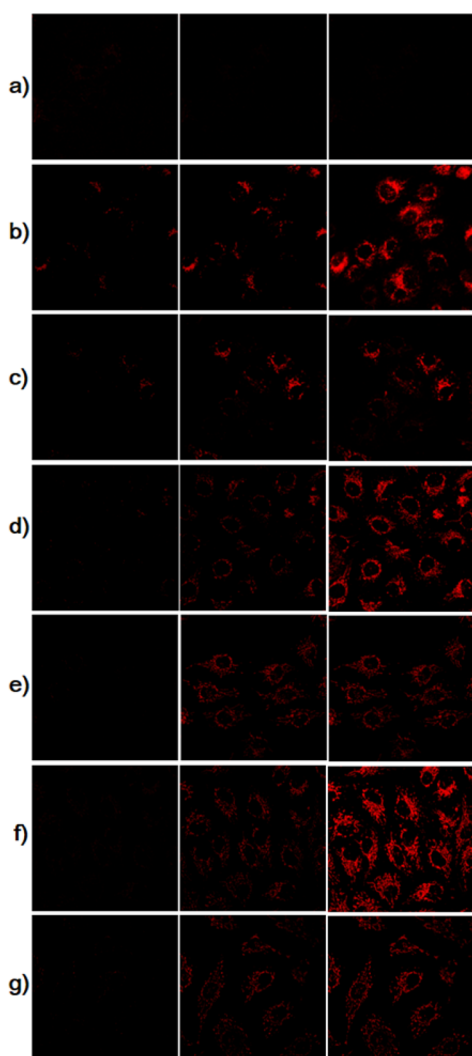


Figure 2. In situ visualization of $\text{O}_2^{\bullet-}$ and H_2S_n level changes in RAW264.7 cells with Hcy-Mito ($1 \mu\text{M}$). Images displayed emission collected windows from 750 to 800 nm upon excitation at 730 nm. a) Incubated with Hcy-Mito as control. b) Manipulated as a), treated with $10 \mu\text{M}$ $\text{O}_2^{\bullet-}$ for 15 min for imaging, then treated with $50 \mu\text{M}$ Na_2S_4 for another 15 min c) After stimulated with $50 \mu\text{M}$ paraquat for 8 h, the cells were incubated with Hcy-Mito for 15 min d) Performed as described in c), the cells were incubated with $50 \mu\text{M}$ H_2S for 30 min e) Described as in d) except the addition of $40 \mu\text{M}$ racemic misonidazole before the addition of $50 \mu\text{M}$ H_2S . f) After incubated with Hcy-Mito for 15 min, the cells were stimulated with $1 \mu\text{g/mL}$ LPS for 30 min, then further cultured for more 16 h. g) Described as in d) but additionally added $100 \mu\text{M}$ PAG.

Hcy-Mito, the cells provided gradual increase in fluorescence indicating the detection of endogenous $\text{O}_2^{\bullet-}$. Glutathione peroxidase (GPx) can scavenge ROS by depleting biotiol. We supposed that GPx could scavenge ROS through converting H_2S to H_2S_n . Next group of cells (Figure 2d) were treated as described in Figure 2c, then $50 \mu\text{M}$ H_2S were added to the cells for 30 min. As expected, remarkable increase in the fluorescence intensity was obtained. However, once inhibited the GPx activity by racemic misonidazole,⁴⁹ the increase in fluorescence emission were suppressed (Figure 2e). These results demonstrated that our probe was suitable for the detection of endogenous $\text{O}_2^{\bullet-}$ and H_2S_n level changes.

It is reported that lipopolysaccharide (LPS) can induce cystathionine γ -lyase (CSE) mRNA overexpression in RAW264.7 cells for promoting the initial real-time production rate of H_2S .⁵⁰ However, LPS can often be employed to quickly stimulate ROS generation in macrophages.⁵¹ We hypothesized that the overexpression of CSE actually triggered by the imbalance of the intracellular redox states. CSE-mediated cysteine metabolism could produce H_2S_n to scavenge the excess ROS.²³ We now verified that the intracellular H_2S_n pool could be perturbed by a $\text{O}_2^{\bullet-}$ burst. The cells in Figure 2f were incubated with Hcy-Mito. After washing with DMEM, the cells were stimulated with $1 \mu\text{g/mL}$ LPS for 30 min. The cells would give red fluorescence response to the generation of $\text{O}_2^{\bullet-}$. These cells were continuously cultured for 16 more hours to prompt endogenous H_2S_n generation. The strong fluorescence emission indicated the high level of endogenous H_2S_n . If the enzyme CSE was inhibited by $100 \mu\text{M}$ PAG,²² as shown in Figure 2g, there was no further enhancement of fluorescence intensity, which revealed that CSE contributed to the H_2S_n generation. The cell body regions in the visual field (Figure 2a–g) were selected as the regions of interest (ROI), and the average fluorescence intensity was shown for the direct contrast-distinction (Figure S10). All these data enabled our probe direct in situ visualization of endogenous $\text{O}_2^{\bullet-}$ and H_2S_n cross-talk in living cells.

Cytoprotection from Cross-Talk between $\text{O}_2^{\bullet-}$ and H_2S_n . H_2S_n is proposed to be more nucleophilic and superior reducing agent for cellular antioxidant activities. The enzyme CSE is considered to be the main source of H_2S_n .²³ It is suggested that H_2S production via CSE is dependent on NADPH oxidase (Nox)-derived H_2O_2 .²² The predominant source of $\text{O}_2^{\bullet-}$ is also dependent on the regulation of Nox. As known, $\text{O}_2^{\bullet-}$ can be immediately converted to H_2O_2 by peroxidase. The long-time burst of $\text{O}_2^{\bullet-}$ in cells would cause cellular oxidative stress and induce apoptosis. We reasoned that this H_2O_2 -related H_2S production should be related to the redox homeostasis between $\text{O}_2^{\bullet-}$ and H_2S_n , which should play an important role in cytoprotection. We now strived to examine the relationship between $\text{O}_2^{\bullet-}$ and H_2S_n in cytoprotection. Human umbilical vein endothelial cells (HUVECs) were employed as test models. As shown in Figure 3, all experimental parallel groups were pre-incubated with $1 \mu\text{M}$ Hcy-Mito for 15 min and washed with DMEM three times before imaging. All the fluorescence responses were further confirmed via flow cytometry assay. Apoptosis induced by cellular oxidative stress was also evaluated. As a control, the cells in Figure 3a emitted no fluorescence. The apoptosis rate in the control cells was almost 0.0%. The treatment of cells with VEGF 40 ng/mL for 15 min would trigger $\text{O}_2^{\bullet-}$ burst (Figure 3b).²² After continuously cultured 30 min, cells in Figure 3b emitted strong fluorescence indicating the rising level of H_2S_n . The rate of apoptosis was 11.5%. Provided per-treated, the cells with $100 \mu\text{M}$ PAG for 10 min to inhibit the activity of CSE, the rate of apoptosis increased up to 20.9% (Figure 3c). As an additional control experiment, treatment with $100 \mu\text{M}$ PAG and $40 \mu\text{M}$ racemic misonidazole for 10 min prompted the apoptosis rate increased to 26.0% (Figure 3d), as PAG and racemic misonidazole could inhibit the activities of CSE and GPx, respectively. The results demonstrated that the main antioxidant activities in HUVECs were attributed to H_2S_n . It was also implied that oxidative stress damage by the burst of $\text{O}_2^{\bullet-}$ could be balanced by the production of H_2S_n . However, the extreme oxidative damage by $\text{O}_2^{\bullet-}$ would lead to collapse of

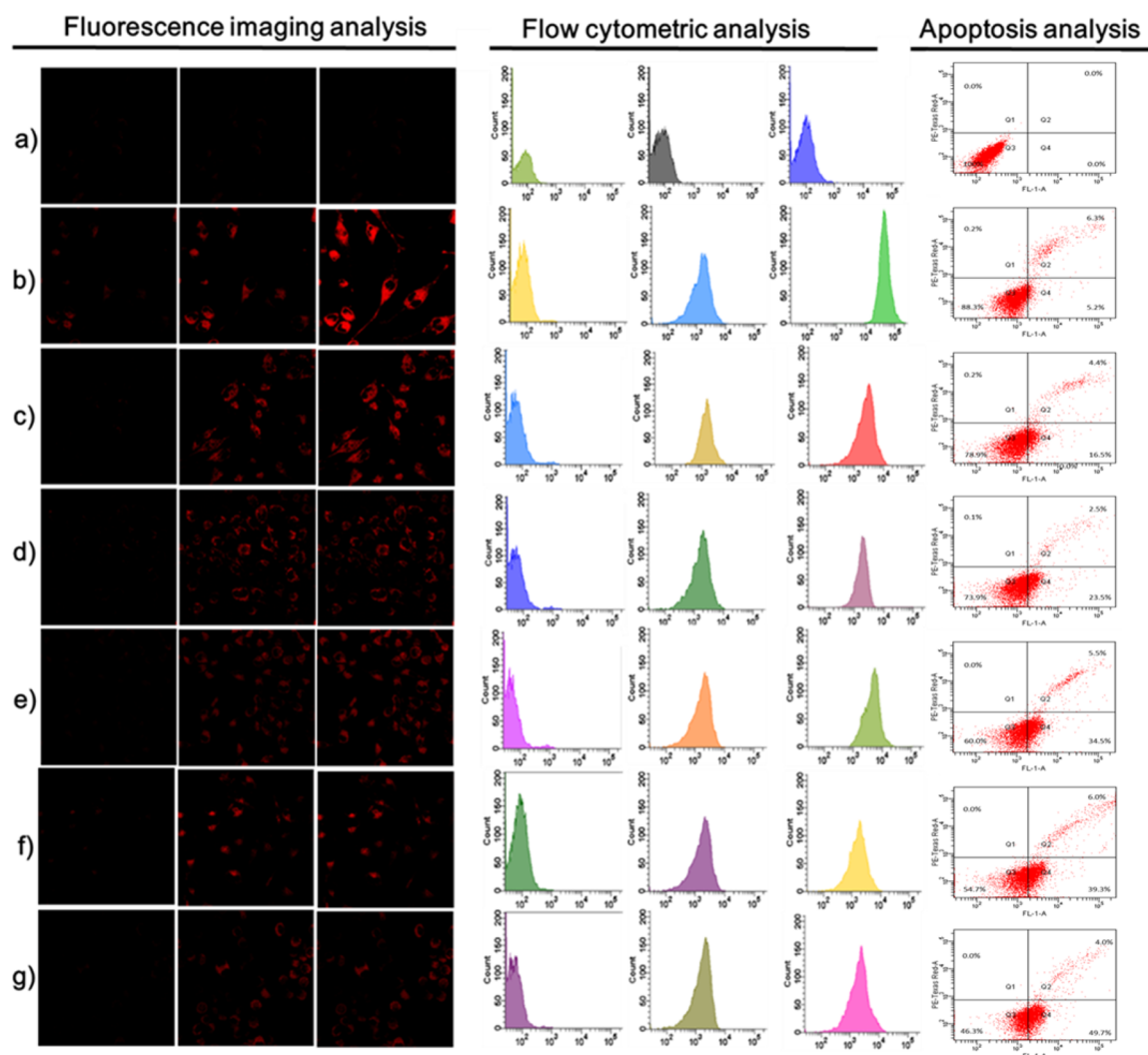


Figure 3. Confocal microscopy images and flow cytometry assay of HUVECs for evaluating the antioxidant activities of H_2S_n . All the cells were incubated with Hcy-Mito ($1 \mu\text{M}$) for 15 min, then washed with DMEM to remove the redundant probe. (a) Control and (b) treated cells with VEGF 40 ng/mL . (c) Performed as described in part b but additionally added PAG $100 \mu\text{M}$. (d) As described in part b but additionally added PAG $100 \mu\text{M}$ and $40 \mu\text{M}$ racemic misonidazole. (e) HUVECs were treated with VEGF 40 ng/mL for 15 min and then incubated with $40 \mu\text{M}$ $\text{O}_2^{\bullet-}$. (f) After treated as indicated as part e, incubated cells with $60 \mu\text{M}$ $\text{O}_2^{\bullet-}$. (g) After treated as indicated as part e, stimulated cells with $80 \mu\text{M}$ $\text{O}_2^{\bullet-}$. The cells imaging and flow cytometry assay time points were at 0, 15, and 30 min. Apoptosis analysis: (Q1) necrotic, (Q2) late apoptosis, (Q3) viable, (Q4) early apoptosis.

antioxidant system. In order to verify excessive $\text{O}_2^{\bullet-}$ could induce serious apoptosis, the assays that directly induced apoptosis by different doses of $\text{O}_2^{\bullet-}$ were performed. HUVECs cells in Figure 3e were treated with VEGF 40 ng/mL for 15 min and then incubated with $40 \mu\text{M}$ $\text{O}_2^{\bullet-}$. Cell imaging illustrated the critical collapse of the antioxidant system, because the weak fluorescence emissions were obtained even at the time point 60 min (Figure S12). The apoptosis rate was 40%. The cells in Figures 3f and 5g were incubated with VEGF 40 ng/mL for 15 min, then treated with doses of 60 and $80 \mu\text{M}$ $\text{O}_2^{\bullet-}$, respectively. All the two group cells displayed low fluorescence. The results indicated that the excess $\text{O}_2^{\bullet-}$ had failed cytoprotective mechanism of H_2S_n . The apoptosis rates were up to 45.3% and 53.7%, respectively.

Detection of $\text{O}_2^{\bullet-}$ and H_2S_n in Mitochondria. Mitochondria are known as the main production source of $\text{O}_2^{\bullet-}$. Mitochondrial oxidative stress can cause cell injury and apoptosis. Therefore, it is crucial to control mitochondrial redox homeostasis. Mitochondria hold approximately 60% of

H_2S_n and their derivatives in cells,^{26,27} which implies the antioxidant and cytoprotective properties of H_2S_n in mitochondria. We next investigated whether Hcy-Mito could in situ detect $\text{O}_2^{\bullet-}$ and H_2S_n in mitochondria. We employed the multicolor colocalization method to confirm whether Hcy-Mito functioned in mitochondria or not. The costaining dyes were mitochondria tracker MitoTracker Green FM and DNA marker Hoechst 33342. Respiratory burst in HUVECs was per-induced utilizing $50 \mu\text{M}$ paraquat for 8 h. After washed with DMEM, cells were loaded with $1 \mu\text{g/mL}$ Hoechst 33342 for 30 min, $1 \mu\text{g/mL}$ MitoTracker Green FM for 15 min and $1 \mu\text{M}$ Hcy-Mito for 15 min. The spectrally separated images acquired from the three dyes were estimated using Image-Pro Plus software. As shown in Figure S15, the probe could respond to $\text{O}_2^{\bullet-}$ within 15 min. Although the images of Cy-Mito and MitoTracker Green FM merged well (Figure S15c), the relatively low fluorescence of Cy-Mito would interfere with the resolution of colocalization. We continued to culture cells until Cy-Mito was reduced and emitted strong fluorescence. As illustrated in

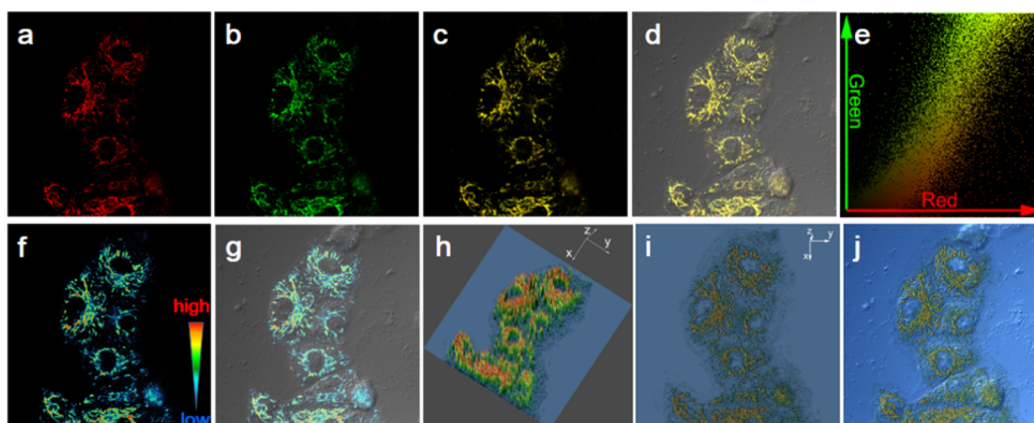


Figure 4. Mitochondrial multicolor colocalization in HUVECs with Hcy-Mito and MitoTracker Green FM. (a) HUVECs cells were treated with 50 μM paraquat for 8 h and then incubated with Hcy-Mito 1 μM for 15 min. Fluorescence imaging of Hcy-Mito at 30 min and (b) fluorescence imaging of MitoTracker Green FM for 15 min, (c) merged red and green channels, (d) merged red, green channels and bright field. (e) Display of the colocalization-correlation between red and green channels in part c; (f) Pseudocolor of part a according to fluorescence intensity profiles. (g) Merged and (f) bright field; surface plots of part a. (h) Perspective observation, (i) vertical view, (j) merged (i) and bright field. Images displayed represent fluorescence emission collected windows: 750–800 nm ($\lambda_{\text{ex}} = 730$ nm) for Hcy-Mito; 500–580 nm ($\lambda_{\text{ex}} = 488$ nm) for MitoTracker Green FM. HUVECs were stimulated with paraquat 1 mM for 8 h, then incubated with 1 μM Hcy-Mito and 1 $\mu\text{g}/\text{mL}$ MitoTracker Green FM for 15 min before imaging.

Figure 4, the cells were stimulated with 50 μM paraquat for 8 h. Then the costaining assays were performed with 1 μM Hcy-Mito and 1 $\mu\text{g}/\text{mL}$ MitoTracker Green FM. After incubation with the dyes for 15 min, the cells were washed with DMEM. The spectrally separated images acquired from the two dyes were constructed at the time point of 30 min. The color-pair intensity correlation analysis for Figure 4a and 6b illustrated high correlated plot between the costaining dyes (Figure 4e). We obtained the Pearson's coefficient $R_r = 0.93$ and the Manders' coefficients $m_1 = 0.95$, $m_2 = 0.96$ implying the preferential distribution of our probe in mitochondria (Figures 4c and 6d). Flow cytometry analysis of mitochondrial isolation for these cells delivered more evidence of our probe targeting in mitochondria (Figure S16). Fluorescence imaging of Figure 4f was additionally presented in pseudocolor according to fluorescence intensity profiles to further identify mitochondrial morphology.⁵² Figure 4g was shown as the plan view. Figure 4h was the perspective observation. Figure 4i was displayed as the vertical view. These imaging analysis convinced that our probe could specifically target in mitochondria for the in situ detection of $\text{O}_2^{\bullet-}$ and H_2S_n level changes successively. The results were of great importance to clarify the physiological relationships between $\text{O}_2^{\bullet-}$ and H_2S_n in cells.

Visualization of $\text{O}_2^{\bullet-}$ and H_2S_n in Vivo. NIR fluorescence facilitates bioimaging in vivo because it can avoid interference from cell autofluorescence, minimize photo damage, and penetrate tissue deeply. The application of Hcy-Mito for fluorescence imaging in vivo was studied in BALB/c mice. As shown in Figure 5, BALB/c mice were divided into three groups. Mice in group a were given intraperitoneal (i.p.) cavity injection with Hcy-Mito (1 μM , 50 μL of 1:99 DMSO/saline v/v) for 20 min as a control. Group b were given i.p. cavity injection with Hcy-Mito for 20 min and then injected with phorbol myristate acetate (PMA) 30 min to induce $\text{O}_2^{\bullet-}$ generation (50 nM, 50 μL in 1:99 DMSO/saline v/v). Group c were pre-treated as indicated in group b. Subsequently, these mice were given an i.p. cavity injection with Na_2S_4 (50 μM , 100 μL in saline) 30 min as the source of H_2S_n . The mice were subjected to imaging on an in vivo imaging system (Bruker). As

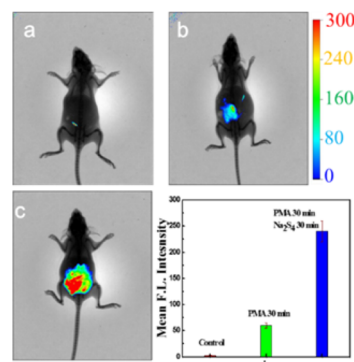


Figure 5. Representative NIR fluorescence imaging for visualizing $\text{O}_2^{\bullet-}$ and H_2S_n in BALB/c mice. (a) Mice were i.p. cavity injected with Hcy-Mito (1 μM , 50 μL in 1:99 DMSO/saline v/v) for 20 min. (b) Mice were loaded with 1 μM Hcy-Mito for 20 min, then injected i.p. with PMA (50 nM, 50 μL in 1:99 DMSO/saline v/v) for 30 min; (c) performed as indicated in group b, then the mice were given i.p. cavity injection with Na_2S_4 (50 μM , 100 μL in saline) for 30 min; (d) mean fluorescence intensity of parts a–c. Images displayed represent emission intensities collected window: 750–850 nm, $\lambda_{\text{ex}} = 735$ nm. (d) Total number of photons from the entire peritoneal cavity of the mice was integrated for quantification. Data are presented as mean \pm SD ($n = 5$).

expected, the control group showed almost no fluorescence. Group b displayed an increase fluorescence indicating that Hcy-Mito responded to $\text{O}_2^{\bullet-}$ in mice. The strong fluorescence in group c suggested that our probe had been reduced by H_2S_n . These results confirmed that the NIR excitation and emission of our probe possessed desirable penetration for successive imaging $\text{O}_2^{\bullet-}$ and H_2S_n in vivo.

The imbalance of $\text{O}_2^{\bullet-}$ and H_2S_n in cells may result in carcinoma. We expected that the probe Hcy-Biot with biotin as targeting group could evaluate the levels of $\text{O}_2^{\bullet-}$ and H_2S_n in cancerous tissue. To explore the targeting effects of Hcy-Biot, the in vivo tumor imaging was performed in xenograft BALB/c mice (murine sarcoma S180 tumor). The level of ROS in cancerous tissue is high. However, the low level of $\text{O}_2^{\bullet-}$ in the

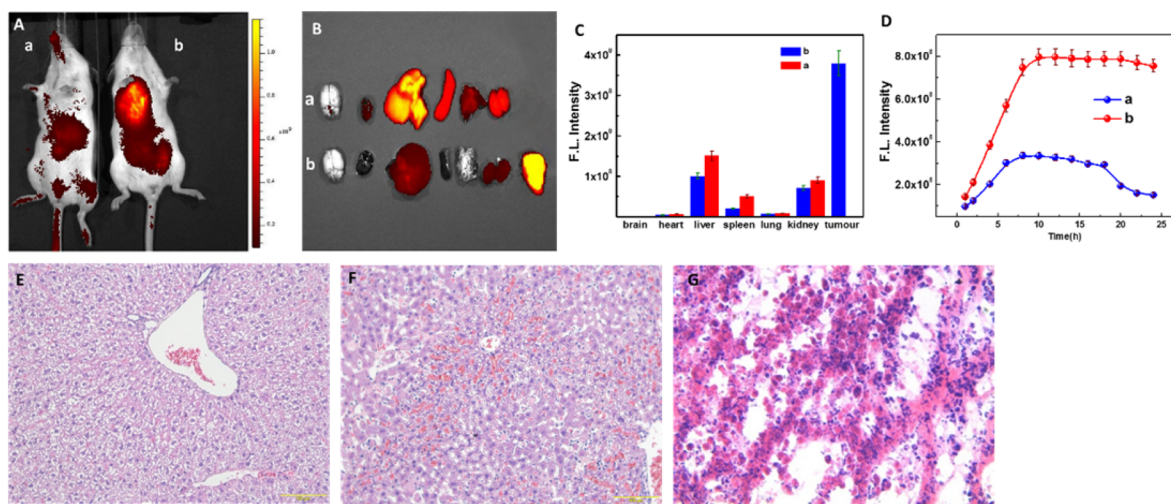


Figure 6. Representative in vivo NIR fluorescence imaging for visualizing $O_2^{\bullet-}$ and H_2S_n . (A) (a) Mice were intravenously injected with 500 mg/kg D-GalN/50 μ g/kg LPS for 24 h, then with intravenous injection of Hcy-Biot (1 μ M, 50 μ L in 1:99 DMSO/saline v/v) for 1 h. (b) The murine sarcoma S180 tumor bearing mice were injected intravenously with Hcy-Biot (1 μ M, 50 μ L in 1:99 DMSO/saline v/v) for 1 h. (B) Organs and tumor tissue of the mice in parts a and b. (C) The fluorescence intensities of organs and tumor tissue in part B. (D) Time-dependent fluorescence intensities after injection of Hcy-Bito. Bioimaging were recorded utilizing the Xenogen IVIS spectrum in vivo imaging system, fluorescence collection window: 750–790 nm with excited wavelength at 730 nm. Data are presented as means \pm SD ($n = 5$); H&E staining of normal liver (F) and acute hepatitis (E). Scale bar: 100 μ m. (E) H&E staining of murine sarcoma S180 tumor ($\times 400$).

healthy mice could not light the fluorescence on within a short time. We induced acute liver injury by D-galactosamine (D-GalN)/LPS in mice for the production of $O_2^{\bullet-}$.⁵³ As shown in Figure 6, the mice in group a were intravenously injected with D-GalN/LPS (500 mg/kg and 50 μ g/kg LPS in saline) for 24 h.

Subsequently, the mice were with intravenous injection of Hcy-Biot (1 μ M, 50 μ L in 1:99 DMSO/saline v/v) and maintained 1 h. The murine sarcoma S180 tumor bearing mice (Figure 6) were injected intravenously with Hcy-Biot (1 μ M, 50 μ L in 1:99 DMSO/saline v/v) for 1 h. Obviously, the liver and tumor tissue could be very quickly distinguished from the surrounding tissues. Fluorescent signal could be maintained even 24 h after the injection (Figure 6D), which demonstrated the targeting delivery and long retention of Hcy-Bito in vivo. The high fluorescence contrasts in Figure 6A were attributed to the depth of liver and tumor tissue (Figure 6B). The penetration depth of Hcy-Bito was at least 1 cm in vivo. H&E (hematoxylin and eosin) staining were carried out to confirm the liver of acute hepatitis and the model of S180 sarcoma tumor (Figure 6E–G). These results indicated that the NIR excitation and emission of our probe possessed desirable penetration depth for in vivo imaging. Ex vivo imaging clearly showed that the selective location of Hcy-Bito was at the tumor tissue over other organs including lung, liver, kidney, heart, spleen, and brain tissue (Figure 6B,C). The results also revealed that high level of $O_2^{\bullet-}$ and H_2S_n might result in the deregulated rapid cell division and proliferation in tumor tissue.

CONCLUSIONS

In summary, we have successfully developed two near-infrared fluorescent probes Hcy-Mito and Hcy-Biot for the detection of $O_2^{\bullet-}$ and H_2S_n in cells and in vivo. As a representative for the examination, Hcy-Mito exhibits outstanding sensitivity and selectivity for endogenous $O_2^{\bullet-}$ and H_2S_n detection. The bioassays in RAW264.7 cells and HUVECs have fully demonstrated that H_2S_n can be prompted to be generated by

mitochondrial oxidative stress. Flow cytometry assays for apoptosis prove that H_2S_n play important roles in antioxidant systems. H_2S_n can protect cells from mitochondrial oxidative stress by direct scavenging $O_2^{\bullet-}$. In vivo NIR fluorescence imaging illustrates that our probes possess desirable penetration depth for imaging $O_2^{\bullet-}$ and H_2S_n in vivo. Moreover, fluorescence imaging of BALB/c mice bearing murine sarcoma S180 tumor demonstrates that Hcy-Biot can target and evaluate $O_2^{\bullet-}$ and H_2S_n in cancerous tissue. We anticipate that the further application of these probes in cells and in vivo will reveal bioroles of $O_2^{\bullet-}$ and H_2S_n in physiological and pathological processes.

ASSOCIATED CONTENT

Supporting Information

The Supporting Information is available free of charge on the ACS Publications website at DOI: 10.1021/acs.analchem.6b00458.

Experimental detail procedures, synthetic procedures and characterization details, reaction kinetics and selectivity, and additional data (PDF)

AUTHOR INFORMATION

Corresponding Authors

*Phone: +86-535-2109130. Fax: +86-535-2109130. E-mail: fbyu@yic.ac.cn.

*E-mail: lxchen@yic.ac.cn.

Notes

The authors declare no competing financial interest.

ACKNOWLEDGMENTS

We thank National Nature Science Foundation of China (NSFC) (Grants 21405172, 21575159, and 21275158) and the program of Youth Innovation Promotion Association, CAS (Grant 2015170).

REFERENCES

- (1) Chen, X.; Tian, X.; Shin, I.; Yoon, J. *Chem. Soc. Rev.* **2011**, *40*, 4783–4804.
- (2) Park, C. M.; Weerasinghe, L.; Day, J. J.; Fukuto, J. M.; Xian, M. *Mol. Biosyst.* **2015**, *11*, 1775–1785.
- (3) Ono, K.; Akaike, T.; Sawa, T.; Kumagai, Y.; Wink, D. A.; Tantillo, D. J.; Hobbs, A. J.; Nagy, P.; Xian, M.; Lin, J.; Fukuto, J. M. *Free Radical Biol. Med.* **2014**, *77*, 82–94.
- (4) Yu, F.; Han, X.; Chen, L. *Chem. Commun.* **2014**, *50*, 12234–12249.
- (5) Lin, V. S.; Chen, W.; Xian, M.; Chang, C. J. *Chem. Soc. Rev.* **2015**, *44*, 4596–4618.
- (6) Chen, W.; Rosser, E. W.; Zhang, D.; Shi, W.; Li, Y.; Dong, W. J.; Ma, H.; Hu, D.; Xian, M. *Org. Lett.* **2015**, *17*, 2776–2779.
- (7) Chen, W.; Rosser, E. W.; Matsunaga, T.; Pacheco, A.; Akaike, T.; Xian, M. *Angew. Chem., Int. Ed.* **2015**, *54*, 13961–13965.
- (8) Gao, M.; Yu, F.; Chen, H.; Chen, L. *Anal. Chem.* **2015**, *87*, 3631–3638.
- (9) Yu, F.; Gao, M.; Li, M.; Chen, L. *Biomaterials* **2015**, *63*, 93–101.
- (10) Gao, M.; Wang, R.; Yu, F.; You, J.; Chen, L. *Analyst* **2015**, *140*, 3766–3772.
- (11) Zeng, L.; Chen, S.; Xia, T.; Hu, W.; Li, C.; Liu, Z. *Anal. Chem.* **2015**, *87*, 3004–3010.
- (12) Paul, B. D.; Snyder, S. H. *Nat. Rev. Mol. Cell Biol.* **2012**, *13*, 499–507.
- (13) Kimura, H. *Antioxid. Redox Signaling* **2014**, *20*, 783–793.
- (14) Linden, D. R. *Antioxid. Redox Signaling* **2014**, *20*, 818–830.
- (15) Wallace, J. L.; Wang, R. *Nat. Rev. Drug Discovery* **2015**, *14*, 329–345.
- (16) Vitvitsky, V.; Kabil, O.; Banerjee, R. *Antioxid. Redox Signaling* **2012**, *17*, 22–31.
- (17) Greiner, R.; Pálkás, Z.; Bäsell, K.; Becher, D.; Antelmann, H.; Nagy, P.; Dick, T. P. *Antioxid. Redox Signaling* **2013**, *19*, 1749–1765.
- (18) Toohey, J. I. *Anal. Biochem.* **2011**, *413*, 1–7.
- (19) Nagy, P.; Winterbourn, C. C. *Chem. Res. Toxicol.* **2010**, *23*, 1541–1543.
- (20) Nagy, P.; Pálkás, Z.; Nagy, A.; Budai, B.; Tóth, I.; Vasas, A. *Biochim. Biophys. Acta, Gen. Subj.* **2014**, *1840*, 876–891.
- (21) Kimura, Y.; Mikami, Y.; Osumi, K.; Tsugane, M.; Oka, J.; Kimura, H. *FASEB J.* **2013**, *27*, 2451–2457.
- (22) Lin, V. S.; Lippert, A. R.; Chang, C. J. *Proc. Natl. Acad. Sci. U. S. A.* **2013**, *110*, 7131–7135.
- (23) Ida, T.; Sawa, T.; Ihara, H.; Tsuchiya, Y.; Watanabe, Y.; Kumagai, Y.; Suematsu, M.; Motohashi, H.; Fujii, S.; Matsunaga, T.; Yamamoto, M.; Ono, K.; Devarie-Baez, N. O.; Xian, M.; Fukuto, J. M.; Akaike, T. *Proc. Natl. Acad. Sci. U. S. A.* **2014**, *111*, 7606–7611.
- (24) Nathan, C.; Cunningham-Bussel, A. *Nat. Rev. Immunol.* **2013**, *13*, 349–361.
- (25) Gorrini, C.; Harris, I. S.; Mak, T. W. *Nat. Rev. Drug Discovery* **2013**, *12*, 931–947.
- (26) Shibuya, N.; Tanaka, M.; Yoshida, M.; Ogasawara, Y.; Togawa, T.; Ishii, K.; Kimura, H. *Antioxid. Redox Signaling* **2009**, *11*, 703–714.
- (27) Jackson, M. R.; Melideo, S. L.; Jorns, M. S. *Biochemistry* **2012**, *51*, 6804–6815.
- (28) Choi, M. G.; Cha, S.; Lee, H.; Jeon, H. L.; Chang, S. K. *Chem. Commun.* **2009**, *47*, 7390–7392.
- (29) Searcy, D. G.; Peterson, M. A. *Anal. Biochem.* **2004**, *324*, 269–275.
- (30) Berube, P. R.; Parkinson, P. D.; Hall, E. R. *J. Chromatogr. A* **1999**, *830*, 485–489.
- (31) Yuan, L.; Lin, W.; Zheng, K.; He, L.; Huang, W. *Chem. Soc. Rev.* **2013**, *42*, 622–661.
- (32) Yu, F.; Li, P.; Wang, B.; Han, K. *J. Am. Chem. Soc.* **2013**, *135*, 7674–7680.
- (33) Yu, F.; Li, P.; Li, G.; Zhao, G.; Chu, T.; Han, K. *J. Am. Chem. Soc.* **2011**, *133*, 11030–11033.
- (34) Zhang, Q.; Zhu, Z.; Zheng, Y.; Cheng, J.; Zhang, N.; Long, Y. T.; Zheng, J.; Qian, X.; Yang, Y. *J. Am. Chem. Soc.* **2012**, *134*, 18479–18482.
- (35) Takahashi, S.; Piao, W.; Matsumura, Y.; Komatsu, T.; Ueno, T.; Terai, T.; Kamachi, T.; Kohno, M.; Nagano, T.; Hanaoka, K. *J. Am. Chem. Soc.* **2012**, *134*, 19588–19591.
- (36) Wrobel, A. T.; Johnstone, T. C.; Deliz, L. A.; Lippard, S. J.; Rivera-Fuentes, P. *J. Am. Chem. Soc.* **2014**, *136*, 4697–4705.
- (37) Liu, J.; Sun, Y.; Huo, Y.; Zhang, H.; Wang, L.; Zhang, P.; Song, D.; Shi, Y.; Guo, W. *J. Am. Chem. Soc.* **2014**, *136*, 574–577.
- (38) Xu, Q.; Lee, K. A.; Lee, S.; Lee, K. M.; Lee, W. J.; Yoon, J. *J. Am. Chem. Soc.* **2013**, *135*, 9944–9949.
- (39) Li, Y.; Wang, H.; Li, J.; Zheng, J.; Xu, X.; Yang, R. *Anal. Chem.* **2011**, *83*, 1268–1274.
- (40) Robinson, K. M.; Janes, M. S.; Pehar, M.; Monette, J. S.; Ross, M. F.; Hagen, T. M.; Murphy, M. P.; Beckman, J. S. *Proc. Natl. Acad. Sci. U. S. A.* **2006**, *103*, 15038–15043.
- (41) Kundu, K.; Knight, S. F.; Willett, N.; Lee, S.; Taylor, W. R.; Murthy, N. *Angew. Chem., Int. Ed.* **2009**, *48*, 299–303.
- (42) Wang, R.; Yu, F.; Chen, L.; Chen, H.; Wang, L.; Zhang, W. *Chem. Commun.* **2012**, *48*, 11757–11759.
- (43) Ueno, T.; Urano, Y.; Kojima, H.; Nagano, T. *J. Am. Chem. Soc.* **2006**, *128*, 10640–10641.
- (44) Presley, A. D.; Fuller, K. M.; Arriaga, E. A. *J. Chromatogr. B: Anal. Technol. Biomed. Life Sci.* **2003**, *793*, 141–150.
- (45) Kumar, R.; Han, J.; Lim, H. J.; Ren, W. X.; Lim, J. Y.; Kim, J. H.; Kim, J. S. *J. Am. Chem. Soc.* **2014**, *136*, 17836–17843.
- (46) Chen, S.; Zhao, X.; Chen, J.; Chen, J.; Kuznetsova, L.; Wong, S. S.; Ojima, I. *Bioconjugate Chem.* **2010**, *21*, 979–987.
- (47) Kimura, H. *Antioxid. Redox Signaling* **2015**, *22*, 362–376.
- (48) Pu, K.; Shuhendler, A. J.; Rao, J. *Angew. Chem., Int. Ed.* **2013**, *52*, 10325–10329.
- (49) Wilde, F.; Chamseddin, C.; Lemmerhirt, H.; Bednarski, P. J.; Jira, T.; Link, A. *Arch. Pharm. (Weinheim, Ger.)* **2014**, *347*, 153–160.
- (50) Zhu, X.; Liu, S.; Liu, Y.; Wang, S.; Ni, X. *Cell. Mol. Life Sci.* **2010**, *67*, 1119–1132.
- (51) Hsu, H. Y.; Wen, M. H. *J. Biol. Chem.* **2002**, *277*, 22131–22139.
- (52) Johnson, L. V.; Walsh, M. L.; Chen, L. B. *Proc. Natl. Acad. Sci. U. S. A.* **1980**, *77*, 990–994.
- (53) Wilhelm, E. A.; Jesse, C. R.; Roman, S. S.; Nogueira, C. W.; Savegnago, L. *Exp. Mol. Pathol.* **2009**, *87*, 20–26.